Implementing Thermal Management Modeling Into SOFC System Level Design

K. J. Kattke
e-mail: kkattke@mines.edu

R. J. Braun[1]
e-mail: rbraun@mines.edu

Division of Engineering,
Colorado School of Mines,
Golden, CO 80401

Effective thermal management is critical to the successful design of small (<10 kW) solid oxide fuel cell (SOFC) power systems. While separate unit processes occur within each component of the system, external heat transport from/to components must be optimally managed and taken into account in system-level design. In this paper, we present a modeling approach that captures thermal interactions among hot zone components and couples this information with system process design. The resulting thermal model is then applied to a mobile SOFC power system concept in the 1–2 kW range to enable a better understanding of how component heat loss affects process gas temperature and flow requirements throughout the flowsheet. The thermal performance of the system is examined for various thermal management strategies that involve altering the convective and radiative heat transfer in the enclosure. The impact of these measures on internal temperature distributions within the cell-stack is also presented. A comparison with the results from traditional adiabatic, zero-dimensional thermodynamic system modeling reveals that oxidant flow requirements can be overpredicted by as much as 204%, resulting in oversizing of recuperator heat duty by 221%, and that important design constraints, such as the magnitude of the maximum cell temperature gradient within the stack, are underpredicted by over 24%. [DOI: 10.1115/1.4002233]

Keywords: SOFC, modeling, system analysis, thermal management

1 Introduction

It is critical to the successful design of small (<10 kW) solid oxide fuel cell (SOFC) power systems that the hot zone enclosure and the components within are designed and packaged in such a way as to minimize heat loss while maintaining thermal self-sufficiency. The typical hardware within SOFC hot zone enclosures includes the fuel cell-stack, fuel processing, heat exchangers, combustors, and piping conduits within which flow process gases, and provides interconnection among system components. While separate unit processes occur within each component, external heat transport from or to components must be optimally managed and taken into account in system-level design. Understanding component interactions and synergistically leveraging heat sinks with heat sources to maintain component and process temperatures are essential aspects of the design, modeling, and simulation process. Modeling the thermal integration of such systems is central to achieving robust design, operability, and high system efficiency.

Modeling the thermofluid transport phenomena within a packaged, high temperature fuel cell system is a complex endeavor that is often tackled by employing a modified commercial computational fluid dynamics (CFD) software for the modeling of the SOFC stack and by ignoring the use of such computationally intensive measures on the balance-of-plant (BoP). Efforts in the extant literature regarding thermal management of entire systems largely focus on dealing with an insulated stack with generic boundary conditions and adiabatic balance-of-plant hardware rather than on capturing interactions of all components in the system with the surroundings [1–5]. The assumption of adiabatic components is largely erroneous as it implies that all of the thermal energy generated within the system due to inefficiencies is convected out via the exhaust gas stream. In fact, for small systems, at least a third or more of the waste heat in the system is rejected via surface heat losses to the surroundings. Additionally, thermal management is often viewed as a strategy of matching process temperatures or selection of cell-stack insulation in order to maintain cell temperature during dynamic operations, such as startup and shutdown [3,6,7]. In this paper, thermal management modeling through low-dimensional modeling techniques is employed in order to provide useful information in system-level process design and operation while avoiding the expensive computational overhead of CFD packages.

2 Objectives and Approach

The overall modeling objective is to investigate the steady-state thermal interactions among components in SOFC systems and to facilitate thermal integration of these components for successful system design. The model allows for system configurations to be evaluated on a thermal management level. Selection of optimal system-level operating parameters is also aided through modeling results. System components include an electrochemical cell-stack, fuel reformer, recuperative heat exchanger, and catalytic burner all packaged within a hot enclosure. The cell-stack is the largest in size of any component in small-scale SOFC systems and its relatively high heat transfer area and high operating temperature cause strong thermal interactions with the smaller balance-of-plant hardware. Thus, one motivation in model development is to capture these effects in order to quantify sensitivity of system processes to SOFC stack operating temperature and design configuration. Considering the dominant role of the cell-stack in thermal management, the modeling strategy focused on enabling feedback of heat transport from/to both the BoP hardware and the SOFC stack.

Details of the developed stack thermal model are presented first, followed by a description of how the stack thermal model is extended to include the BoP components. The resulting thermal

[1]Corresponding author.

Contributed by the Advanced Energy Systems Division of ASME for publication in the JOURNAL OF FUEL CELL SCIENCE AND TECHNOLOGY. Manuscript received May 27, 2010; final manuscript received July 2, 2010; published online November 30, 2010. Editor: Nigel M. Sammes.

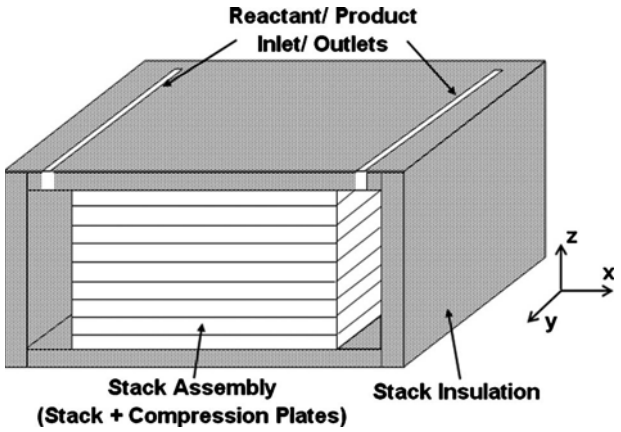

Fig. 1 Stack module cut view

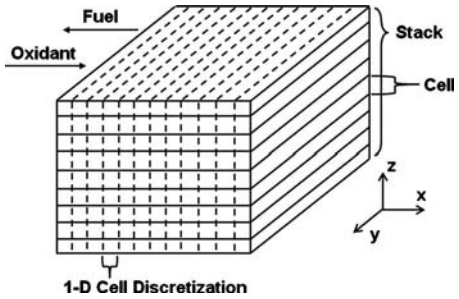

Fig. 2 Counterflow 1D planar stack model

model of the plant is connected to a system-level thermodynamic process design model to enable a better understanding of how component heat loss affects process gas temperatures and flow requirements throughout the flowsheet. The resulting model is exercised on an ~1 kW SOFC system intended for mobile power applications. System performance sensitivity is examined for various thermal management strategies that involve altering the convective and radiative heat transfer in the enclosure. The impact of these measures on internal temperature distributions within the cell-stack is also studied.

3 SOFC Stack Module Thermal Model

The objective of SOFC stack thermal modeling is to estimate the module surface heat loss that inevitably occurs but is not captured by the typical assumption of adiabatic stack operation. The planar stack module thermal model begins with a simplified view of the stack assembly (repeating cell units, compression plates, and manifolding) and the insulation that is wrapped around the stack assembly, as shown in Fig. 1. The stack under investigation is in a counterflow arrangement, but the methodology given herein could easily be applied to coflow configurations. Reactant and product gases enter the stack module through slots in the insulation and distribute inside manifolds before entering the anode/cathode flow channels. In practice, the internal manifolding of the stack separates anode and cathode streams in much the same way as a counterflow plate-fin heat exchanger, but in this simplified viewpoint, the manifold is considered an open volume where separation of oxidant and fuel streams is ignored. This is a valid assumption in that separation of the streams occurs with high thermal conductivity metals.

The stack module geometry in Fig. 1 yields four sides of the stack assembly that are in intimate contact with insulation and two stack assembly sides, which are adjacent to the gas manifolds. These six stack assembly sides represent the internal thermal boundary conditions for the stack module thermal model. The thermal boundary conditions are specified by stack boundary temperatures calculated with a previously developed [8,9] 1D planar cell model that is incorporated within the thermodynamic system model. A schematic of the stack without manifolding and insulation is given in Fig. 2 and includes the discretization of the 1D model in the direction of reactant gas flow.

Solution to the 1D cell model yields a streamwise temperature profile. In this stack modeling approach, the performance of a single cell is aggregated to represent the entire stack, resulting in a streamwise stack temperature profile (i.e., along x in Fig. 2) and no temperature gradients normal to stack gas flows (along y and z in Fig. 2). Beale [5] developed a reduced order distributed resistance analogy model to study a cross-flow stack with rectangular manifolding. While Beale considered an adiabatic stack package, it was found that the gases in the stack inlet and outlet manifolds did not register significant temperature gradients along the z axis (see Fig. 1). Beale's results supported the use of a 1D stack model in the present study. With the existence of a streamwise temperature profile, it would be inaccurate to use a single average surface temperature to represent the six sides of the stack. To increase the thermal model fidelity of the stack module, the outer insulation skin of the stack module is divided into three surfaces, which can be at varying temperatures (see Fig. 8).

A lumped, area-averaged cell temperature is assumed at the four stack assembly surfaces that are in intimate contact with stack insulation, i.e., the four external stack surfaces that are not exposed to inlet/exit manifold gas flows (note that this approach assumes the top and bottom compression plates are also at same temperature as the stack). The validity of this approach was tested by comparing the area-averaged surface heat flux with the discretized surface heat flux at the stack periphery. The surface heat flux using the area-averaged cell temperature was observed to be within 0.2% of the discretized surface for a given ambient temperature.

The remaining two sides of the stack serve as the reactant gas inlets/outlets to the repeating cell elements and are adjacent to the gas manifolds. High SOFC operating temperatures point to radiation as a substantial heat transfer mechanism; therefore, this mode is combined with convection inside the manifolds. Radiation heat exchange in a manifold is assumed to occur between the five insulation surfaces and the adjacent stack side that make up the manifold enclosure (see Fig. 3). All surfaces are assumed opaque, diffuse, and gray. Slots in the insulation for reactant/product gases entering the manifold are relatively small and are added to the top surface area of the manifold, creating a complete enclosure. The end surfaces of the stack adjacent to the manifold (i.e., at $x=0$ and $x=L$ in Fig. 2) are composite surfaces composed of cell trilayers (cathode-electrolyte-anode/anode support), interconnects, gas flow channels, and compression plates, as shown in Fig. 4. Rather than

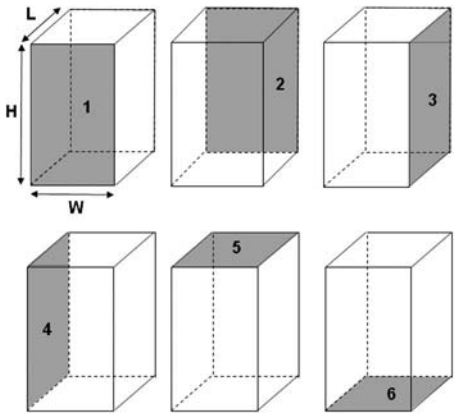

Fig. 3 Stack module manifold enclosure with surface numbers

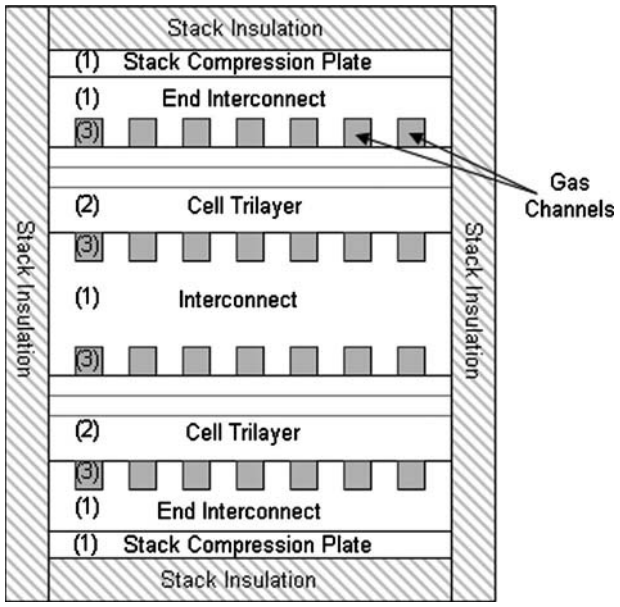

Fig. 4 Two cell-stack assembly as viewed from gas manifold

discriminate between each trilayer surface inside the gas distribution manifold, all stack trilayers are lumped into a single surface. Similarly, each interconnect in the stack is lumped into a single interconnect surface and each cell gas channel is lumped into a single gas channel surface. Because of small areas and view factors relative to the manifold enclosure, gas flow channels are assumed to be irradiating surfaces. Compression plates are lumped into the interconnect surface because of comparable radiation properties due to similar metallic construction materials. This yields eight surfaces comprising the cavity enclosure (five insulation surfaces and one stack surface that is decomposed into three separate surface areas).

The manifold heat transfer model begins with temperature boundary conditions provided by the cell model at the inlet/outlet of the cell. Cross-plane temperature differences of less than 1 °C in SOFCs [10] allow for the cell trilayer temperature to be lumped in the 1D cell model. The interconnect temperature is also resolved; therefore, the 1D model yields two temperature profiles, a trilayer and an interconnect profile. This results in two surface boundary temperatures at the stack sides adjacent to the manifolds.

Enclosure view factors are calculated using relations for aligned parallel rectangles and perpendicular rectangles with a common edge [11] and are summarized in Table 1.

Surface 3 in Fig. 3 serves as the composite cell surface in the left manifold and is comprised of irradiating gas channels, radiating trilayers, and radiating interconnects/compression plates. As discussed earlier, all stack trilayers are lumped into a single trilayer surface (surface 2 in Fig. 4). The same lumping procedure follows for interconnects and gas channels (surfaces 1 and 3, respectively, in Fig. 4). Because trilayers, interconnects, and gas channels are tightly spaced and repeated throughout the stack, the view factors for the composite surface are computed as follows.

Table 1 Manifold enclosure view factors F_{ij}

		i					
		1	2	3	4	5	6
j	1	0.000	0.031	0.039	0.039	0.052	0.052
	2	0.031	0.000	0.039	0.039	0.052	0.052
	3	0.462	0.462	0.000	0.891	0.446	0.446
	4	0.462	0.462	0.891	0.000	0.446	0.446
	5	0.022	0.022	0.016	0.016	0.000	0.005
	6	0.022	0.022	0.016	0.016	0.005	0.000

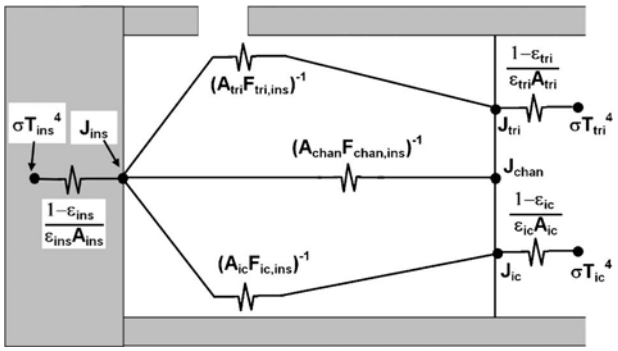

Fig. 5 Radiation resistance model (composite stack surface and adjacent insulation manifold surface radiation exchange shown)

From stack composite surfaces to manifold insulation surfaces,

$$F_{\text{tri},j} = F_{ic,j} = F_{\text{chan},j} = F_{3,j} \tag{1}$$

From manifold insulation surfaces to stack composite surfaces,

$$F_{j,\text{tri}} = \frac{A_{\text{tri}}}{A_3} \cdot F_{j,3} \tag{2}$$

$$F_{j,ic} = \frac{A_{ic} + A_{\text{comp plates}}}{A_3} \cdot F_{j,3} \tag{3}$$

$$F_{j,\text{chan}} = \frac{A_{\text{chan}}}{A_3} \cdot F_{j,3} \tag{4}$$

where $F_{j,i}$ is the view factor from surface j to i and A_i is the surface area of surface i.

Focusing on a single manifold, radiosity balances on all eight manifold surfaces produce a set of equations in which surface radiosities are calculated.

For radiating surfaces i,

$$\frac{\sigma T_i^4 - J_i}{\frac{1-\varepsilon_i}{\varepsilon_i A_i}} = \sum_{j=1}^{8} \frac{J_i - J_j}{(A_i F_{ij})^{-1}} \tag{5}$$

For irradiating gas channel surface i,

$$0 = \sum_{j=1}^{8} \frac{J_i - J_j}{(A_i F_{ij})^{-1}} \tag{6}$$

where J_i is the radiosity at surface i and ε_i is the emissivity of surface i.

Net radiation heat transfer leaving each surface in the manifold is calculated as

$$\dot{Q}_{\text{rad},i} = \frac{\sigma T_i^4 - J_i}{\frac{1-\varepsilon_i}{\varepsilon_i A_i}} \tag{7}$$

The lumped thermal radiation resistance model for the left manifold in Fig. 1 is shown in Fig. 5. For simplicity, radiation exchange is only shown between the composite stack surface and the manifold surface parallel to the stack. An equivalent radiation resistance network models the interactions between all surfaces in each manifold enclosure. In total, there are eight surfaces per manifold: five manifold insulation surfaces and three lumped surfaces representing the face of the cell-stack (trilayers, interconnects, and gas channel openings).

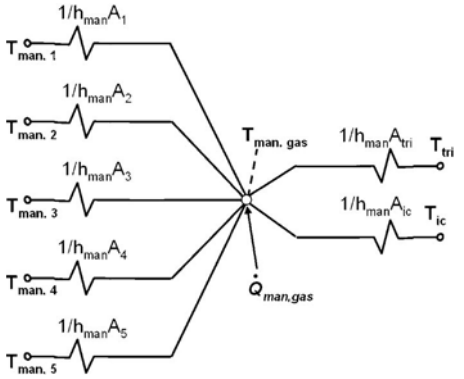

Fig. 6 Manifold convection resistance network

Convective heat transfer is modeled in the manifold using the same eight lumped surface temperatures minus the gas channels, as in the radiation model. Heat transfer due to convection leaving each surface i is calculated by

$$\dot{Q}_{\text{conv},i} = h_{\text{man}} A_i (T_i - T_{\text{man,gas}}) \tag{8}$$

where A_i is the surface area, T_i is the temperature of surface i, h_{man} is the heat transfer coefficient, and $T_{\text{man,gas}}$ is the temperature of the stack manifold gas.

Assuming a perfectly mixed condition inside the cavity, the amount of heat added to the resistance network is calculated as

$$\dot{Q}_{\text{man,gas}} = \dot{m}_{\text{man,gas}} \cdot cp_{\text{man,gas}} (T_{\text{gas,in}} - T_{\text{man,gas}}) \tag{9}$$

where $\dot{Q}_{\text{man,gas}}$ is the thermal energy transported from manifold gas, $\dot{m}_{\text{man,gas}}$ is the flow rate in a stack manifold, $cp_{\text{man,gas}}$ is the heat capacity, $T_{\text{man,gas}}$ is the temperature of the manifold gas, and $T_{\text{gas,in}}$ is the temperature of gases entering the manifold.

Oxidant flow is generally an order of magnitude greater than fuel flow in SOFCs; therefore, the mass flow rate and temperature of oxidant (not the fuel) is used in Eq. (9). At the oxidant inlet manifold of the stack module, $T_{\text{gas,in}}$ is the oxidant temperature entering the stack module and $T_{\text{man,gas}}$ is the temperature of oxidant entering the cathode compartment of the cell. At the oxidant outlet manifold of the stack module, $T_{\text{gas,in}}$ is the oxidant temperature leaving the cathode and $T_{\text{man,gas}}$ is the oxidant temperature leaving the stack module.

A convection resistance network for the left manifold in Fig. 1 is shown in Fig. 6 using the surface numbering scheme of Fig. 3. An equivalent network is written for the right manifold.

Energy balances on each manifold surface combine the radiation and convection resistance models and results in the amount of thermal energy entering each surface,

$$\dot{Q}_{\text{in},i} = -(\dot{Q}_{\text{rad},i} + \dot{Q}_{\text{conv},i}) \tag{10}$$

Thermal energy leaving the interconnect and trilayer surfaces at the manifold is evenly distributed as a heat flux boundary condition to the interconnect and trilayer energy balances at the inlet/outlet of the 1D cell model. Conductive heat transfer leaving the four sides of the stack in intimate contact with insulation is calculated using the streamwise average stack temperature as shown in Fig. 7. Conduction leaving the stack is evenly distributed as a heat flux boundary condition to the cathode gas channel energy balance at all interior cell control volumes. Conduction heat transfer is removed from the cathode gas channel because in SOFCs, convective cathode gas cooling is the dominate stack cooling method.

As stated earlier, the exterior of the stack module is modeled as three separate surfaces. However, the interior of the stack module contains 11 inner stack module insulation surfaces that connect to the exterior surfaces via the conductive heat transfer resistance network depicted in Fig. 7. The 11 inner insulation surfaces consist of five surfaces per manifold and a single insulation surface where the stack is in intimate contact with the insulation. In the resistance network shown, right refers to the right manifold and left refers to the left manifold in Fig. 1. The outer insulation skin is comprised of three lumped temperature surfaces (A, B, and C), as shown in Fig. 8. The three surfaces depicted are the two shaded end surfaces B and C along with the four unshaded insulation sides that comprise the third surface, A. Assuming three outer insulation surfaces results in less than a 0.10% difference in total stack module heat loss compared with using 11 outer insulation surfaces as done at the inner skin of the insulation. The three stack insulation skin temperatures are connected to the overall SOFC system thermal model, as described in Sec. 4.

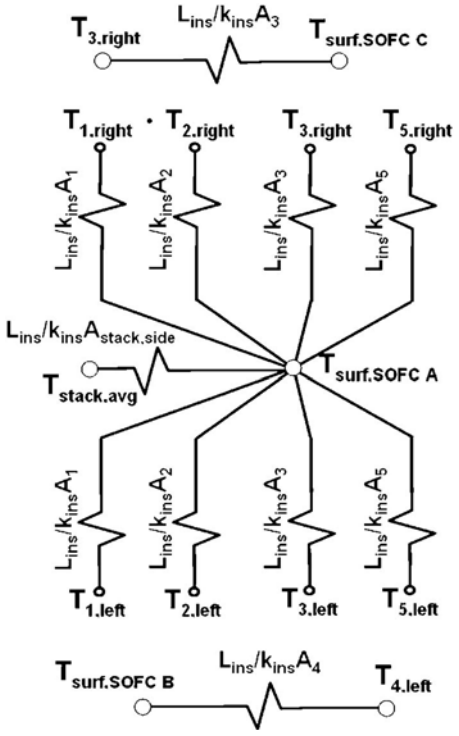

Fig. 7 Stack insulation conduction model

3.1 Summary of Stack Model Assumptions and Impacts. Assumptions made in development of the SOFC stack thermal model are summarized below.

1. Extrapolation of single-cell performance as predicted by 1D model for entire stack and uniformly distributed reactant gases are assumed.

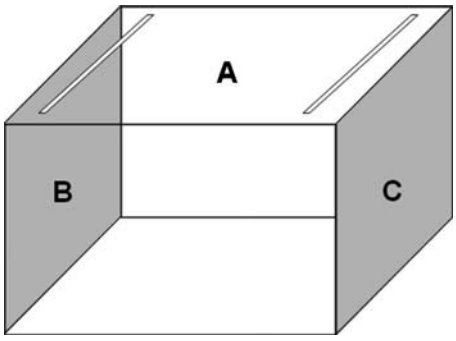

Fig. 8 External surfaces of insulated stack assembly

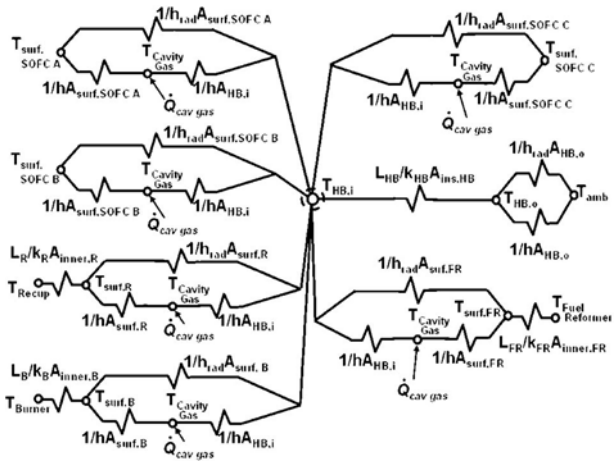

Fig. 9 SOFC system thermal resistance model

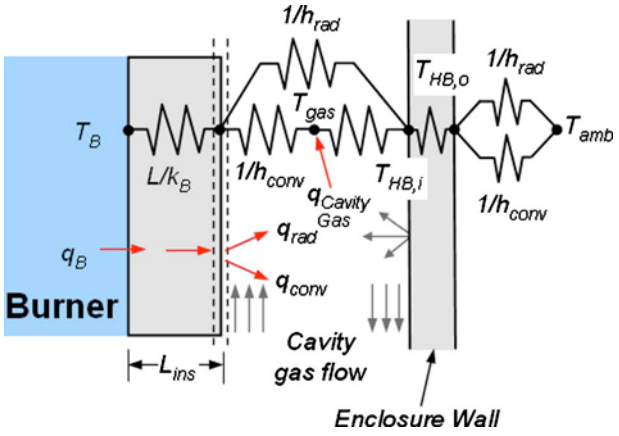

Fig. 10 Burner resistance model connection to ambient temperature outside of enclosure

2. Radiation exchange in gas manifolds assumes opaque, diffuse, and gray surfaces with nonemitting transparent gases.
3. Internal manifolding separating anode and cathode streams neglected due to its high thermal conductivity.
4. Cell repeating trilayers, interconnects, and gas channels are lumped to form three surfaces in each manifold.
5. Gas channels are considered irradiating surfaces due to relatively small view factors and areas with respect to remaining manifold surfaces.
6. Reactant gases are perfectly mixed in manifolds with the dominant reactant flow assumed to be that of cathode gas flow.
7. Fuel flow within the stack manifolds is considered to be adiabatic.

Utilizing a 1D stack model does not lend itself to identifying localized stack hot/cold zones but this approach is sufficient in predicting nominal stack performance characteristics, temperature gradients, and heat rejection. Larger localized temperature gradients are likely to arise than predicted by this model but experimental knowledge would allow for appropriate scaling factors to be applied in predicting higher localized gradients. Neglecting detailed internal manifolding geometry allows radiation view factors to be calculated with relative ease but is expected to result in an overprediction of radiation heat transfer because internal manifolding is an additional resistance to radiation thermal energy exchange. Lumping of stack repeating surfaces in each manifold is appropriate for a 1D stack model. Anode gas flow is excluded in manifold gas mixing because anode flow is an order of magnitude less than cathode flow; its exclusion has little impact on thermal capacity and temperature of cavity gases. Perfectly mixed manifold gas is supported by previous work where the largest temperature difference in similar rectangular manifolds was seen to be 26°C [5].

4 System Thermal Model

A thermal model of the SOFC system components within the hot enclosure (see Fig. 9) was also developed for a power system representative of mobile and small stationary applications. The system thermal model assumes a lumped, uniform surface temperature for all balance-of-plant components and enclosure surfaces and accounts for conduction, convection, and radiation heat transfer mechanisms. The SOFC stack is comprised of three surface temperatures, as described above and shown in Fig. 8. System piping is assumed insulated and adiabatic except in the fuel piping, most notably between the reformer (catalytic partial oxidation (CPOx) unit) and the SOFC. Convection heat transfer occurs between system components and the enclosure (or hot box) cavity gas as well as radiation heat transfer between system components and the enclosure inner wall. Importantly, component-to-component radiative interactions are assumed negligible compared with the interaction between a single component and the surrounding enclosure walls and cavity gas. The validity of this assumption is largely dependent on system packaging. The more closely the components are packaged next to one another (i.e., high packing efficiencies[2]), the more consideration must be given to component interactions. The net heat transfer from BoP components is written in terms of a temperature difference divided by the overall resistance as follows:

$$\dot{Q}_{\text{total},i} = \frac{T_i - T_{\text{skin},i}}{R_{\text{ins},i}} \tag{11}$$

$$\dot{Q}_{\text{conv},i} = \frac{T_{\text{skin},i} - T_{\text{cav,gas}}}{R_{\text{conv},i}} \tag{12}$$

$$\dot{Q}_{\text{rad},i} = \frac{T_{\text{skin},i} - T_{HB,i}}{R_{\text{rad},i}} \tag{13}$$

$$\dot{Q}_{\text{total},i} = \dot{Q}_{\text{conv},i} + \dot{Q}_{\text{rad},i} \tag{14}$$

where $\dot{Q}_{\text{total},i}$ is the rate of heat transfer from component i, T_i is the lumped inner wall surface temperature of component i, $T_{\text{skin},i}$ is the insulation surface temperature of component i, $T_{\text{cav,gas}}$ is the hot box cavity gas temperature, and $T_{HB,i}$ is the inner hot box surface temperature. The net heat transfer rate from the SOFC stack is similarly calculated using the surface temperatures calculated in the stack thermal model, where Eqs. (12) and (13) are written for the three stack skin surfaces.

Figure 10 provides an example illustration of the details of the thermal resistance network model between the catalytic burner and the surroundings. Heat is transmitted via conduction through the skin material of the burner. Surface heat flux from the outer surface of the component reflects the combined modes of radiation and convection heat transfer. Radiation heat flux between the burner outer skin surface and the enclosure assumes gray diffuse surfaces with an assumed view factor of 1.0 and a linearized radiation heat transfer coefficient.

The equivalent heat transfer resistance for the burner is expressed as

[2]"High" packing efficiencies are typically >65% where packing efficiency is defined as the sum of component volumes divided by the total enclosure volume.

$$R_{\text{tot},B} = \frac{L_B}{k_B A_{B,i}} + \frac{1}{h_{\text{rad},B} A_{B,o} + \left(\frac{1}{h_{\text{conv},B} A_{B,o}} + \frac{1}{h_{\text{conv},HB} A_{HB,i}} \right)^{-1}}$$

$$+ \frac{L_{HB}}{k_{HB} A_{HB,i}} + (h_{\text{conv,amb}} A_{HB,o} + h_{\text{rad,amb}} A_{HB,o})^{-1} \quad (15)$$

A thermal resistive network for the entire hot box can be developed from this basic framework by coupling each of the components to the inner hot box wall temperature $T_{HB,i}$ and the cavity gas temperature $T_{\text{cav,gas}}$. Figure 9 depicts the resistive network for the entire SOFC system thermal model. Components in the hot box include the SOFC stack, catalytic burner, CPOx reformer, and recuperator. Balance-of-plant components within the hot box approximate their inner wall surface temperature by taking an average gas temperature. The small resistance associated with the metallic wall thickness compared with insulation resistance of the component is neglected. The stack surface temperatures are outputs from the stack thermal model. While components are not *directly* coupled to one another via radiation mechanisms, they are coupled through convection at the cavity gas temperature by applying an energy balance to the hot box cavity gas node

$$\sum_i \dot{Q}_{\text{conv,BoP},i} + \sum_i \dot{Q}_{\text{conv,stack},i} + \dot{Q}_{\text{conv},HB,i} + \dot{Q}_{\text{cav,gas}} = 0 \quad (16)$$

System configurations arise where stack exhaust gases, leaving the recuperator may be circulated inside the hot enclosure before being plumbed out of the enclosure. To allow for circulating cavity gas flow, a perfectly mixed condition inside the enclosure is considered where the amount of heat added to the resistance network is calculated as

$$\dot{Q}_{\text{cav gas}} = \dot{m}_{\text{cav.gas}} \cdot cp_{\text{cav.gas}} (T_{\text{gas in}} - T_{\text{cav.gas}}) \quad (17)$$

where $\dot{m}_{\text{cav.gas}}$ and $T_{\text{gas in}}$ are the states of exhaust leaving the recuperator, $T_{\text{cav.gas}}$ is the temperature of cavity gases within the hot enclosure, and $cp_{\text{cav.gas}}$ is the average specific heat calculated at the inlet and cavity gas temperatures.

Components are also coupled through radiation by a common interaction with the inner surface of the enclosure wall. This coupling is achieved by applying an energy balance to the hot box inner wall node as follows:

$$-\dot{Q}_{\text{conv},HB,i} + \sum_i \dot{Q}_{\text{rad,BoP},i} + \sum_i \dot{Q}_{\text{rad,stack},i} = \dot{Q}_{HB,\text{out}} \quad (18)$$

$$\dot{Q}_{\text{conv},HB,i} = \frac{T_{HB,i} - T_{\text{cav,gas}}}{R_{\text{conv},HB,i}} \quad (19)$$

$$\dot{Q}_{HB,\text{out}} = \frac{T_{HB,i} - T_{\text{amb}}}{R_{\text{ins},HB} + R_{\text{amb}}} \quad (20)$$

where $\dot{Q}_{HB,\text{out}}$ is the rate of heat transfer leaving the hot box to the surroundings and R_{amb} is the heat transfer resistance from the hot box outer skin to the surroundings; it can include any combination of radiation and convection.

4.1 Summary of System Model Assumptions and Impacts. Assumptions made in development of the system-level thermal model are summarized below.

1. BoP (not including stack) surface temperatures are lumped and predicted by the average inlet and outlet gas streams of each respective component.
2. Radiation exchange only occurs between each system component and the hot box itself, i.e., no component-to-component radiation exchange.
3. Each component "sees" the hot box inner wall with a view factor of 1.0.

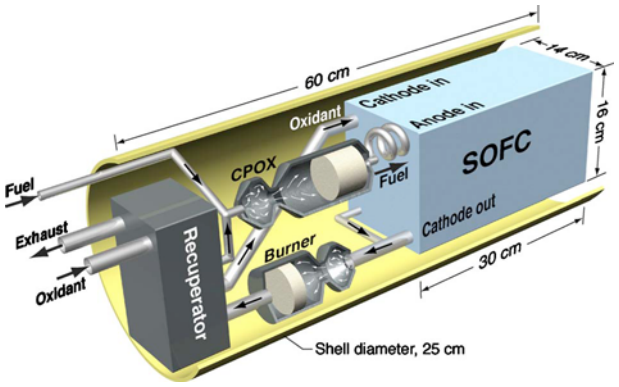

Fig. 11 Representative planar SOFC system

4. Surfaces are opaque, diffuse, and gray and utilize a linearized radiation heat transfer coefficient.
5. Cavity gas circulation is assumed to be perfectly mixed and the gases are assumed to be transparent in the infrared spectrum.
6. Heat loss associated with conduction from enclosure piping and instrumentation penetrations is neglected.

Using component view factors of 1.0 assumes a relatively large hot box area in comparison to component areas. In the case of larger system components, i.e., the stack and the recuperator, where the hot box sees the component, radiation exchange from larger components is expected to be overpredicted. The source of the cavity gas flow is envisioned to be the exhaust from the recuperator. Thus, heat transfer from components near the inlet of cavity gases into the enclosure will experience the greatest error since that is where the largest departure from the perfectly mixed temperature occurs. Lumped surface temperatures and lack of component-to-component radiation exchange will tend to underpredict the coupling of neighboring system components. Greater fidelity in capturing component-to-component interactions requires either a more elaborate 1D system model or the use of computational fluid dynamics.

5 System Description

The system thermal model was integrated into a thermodynamic system process design model to capture interactions between component heat loss or gain and process gas temperatures and flow conditions. The predictive nature of the resulting integrated model provides feedback to system design parameters such as component sizing and required flow rates. The model is exercised on a 1.1 kW (gross) mobile SOFC system shown in Fig. 11. The figure illustrates the general layout of the system where each unit operation is a discrete component. The SOFC stack is supported by a dielectric at its corners with a press fit between the stack and the enclosure inner wall. This example SOFC system concept is intended for unmanned underwater vehicle (UUV) applications, but the essential features of the integrated thermal system model are applicable to many other similar-sized applications. The external boundary condition on the hot box can take many forms depending on the UUV configuration. In this study, the enclosure is wrapped in a metal liner and insulation packaged within the vehicle hull. The surrounding environment of the enclosure can vary, but in this study, the outer enclosure surface is envisioned to be in direct contact with ocean water. Assuming conduction resistance through the metal liner is negligible and the ocean water is opaque, the external boundary condition on the hot box is purely convective.

Ambient conditions surrounding the hotbox are representative of ocean water at a depth of 10 m (P_{amb}=2.023 bars) and a temperature of 20°C.

Table 2 Planar SOFC system geometry

	Stack assembly	Stack module	Recuperator	CPOx	Burner	Enclosure
Height (cm)	28.0	30.0	9.6	N/A	N/A	N/A
Width (cm)	12.0	14.0	7.1	N/A	N/A	N/A
Length (cm)	12.0	16.0	17.2	16.2	10.4	60.0
OD (cm)	N/A	N/A	N/A	4.8	4.1	25.0
Ins. thick. (mm)	10.0	10.0	10.0	5.0	1.0	10.0
Ins. material	fb/aerogel	fb/aerogel	aerogel	fb	fb	aerogel

Unlike the thermodynamic system model, representative geometry is required in the thermal model. The system geometries are listed in Table 2. Stack cells are 10×10 cm^2 in size and stack manifolds are 1 cm in width.

Each component in the thermal model is wrapped in either high temperature Microtherm™ fiberboard or lower temperature aerogel insulation with empirical fits [12] of the temperature dependence of thermal conductivity given below in Eqs. (21) and (22) where T is in °C. The SOFC insulation is comprised of a first layer of fiberboard and a second layer of aerogel, both of equal thickness.

$$k_{fb} = 2.14E^{-2} + 1.2857E^{-5}T + 2.8571E^{-8}T^2 \tag{21}$$

$$k_{\text{aerogel}} = 9.7486E^{-3} + 5.7E^{-4}T - 2.1429E^{-8}T^2 \tag{22}$$

Baseline convective heat transfer coefficients for the system are listed in Table 3. In this system, the external heat transfer coefficient for each BoP component, the SOFC stack, and the enclosure inner wall is assumed equal to h_{HB} (W/m^2 K). A forced and natural convection baseline h_{HB} is used depending on whether gases are circulated inside the enclosure. The natural convection coefficient was calculated using a natural convection relationship for a long horizontal cylinder with the burner geometry. The forced convection heat transfer coefficient is a design/operating parameter because it can be increased above its lower bound by installing a high temperature circulating fan in the enclosure or injecting recuperator exhaust gas into the enclosure. The lower bound of the convective heat transfer coefficient at the external wall of the enclosure h_{amb} is calculated using a free convection relationship for a long horizontal cylinder with the enclosure geometry. The heat transfer coefficient h_{amb} is also an operating parameter as it increases above the free convection baseline as speed of the UUV through the water increases.

The heat transfer coefficient in the stack manifolds was calculated using a duct flow Nusselt number relationship using the average oxidant mass flow rate in a manifold and a flow area equal to 80% of the flow area in the manifold, which takes into account fuel flow through approximately 20% of the manifold. The average oxidant manifold mass flow rate equals 1/2 of the mass flow rate entering the manifold, assuming oxidant is equally distributed to all gas channels in the stack.

There are two heat transfers in the SOFC system that are calculated with the thermodynamic system model. Thermodynamically required heat transfer is used to preheat fuel prior to entering the CPOx reformer and to remove energy from the CPOx reformate (see Fig. 12). The relatively low energy input to preheat is taken directly from the heat rejected from the CPOx reformate. The amount of CPOx reformate heat remaining after removing energy for fuel preheat is added to the enclosure resistance model. Physically, the CPOx reformate rejects thermal energy through convection and radiation to the enclosure during pipe flow from the CPOx to the stack anode inlet. Since piping geometry is unknown, the thermodynamically required CPOx reformate heat loss is added to the resistance model. By applying the reformate average gas temperature out of the CPOx and into the stack to a cylindrical pipe geometry, it was determined that 55% of CPOx reformate heat loss is associated with radiation heat transfer and 45% is associated with convection heat transfer. The radiative CPOx reformate gas heat loss is added to the resistance model by adding the following to the $T_{HB,i}$ node.

$$\dot{Q}_{\text{rad,CPOx ref}} = 0.55(\dot{Q}_{\text{CPOx ref total}}) \tag{23}$$

The convective CPOx exhaust heat loss is added to the resistance model by adding the following to the $T_{\text{cav gas}}$ node.

$$\dot{Q}_{\text{conv,CPOx ref}} = 0.45(\dot{Q}_{\text{CPOx ref total}}) \tag{24}$$

Surface emissivity values are shown in Table 4. Both insulation materials are assumed to have equal emissivity values. Stack manifolds have an emissivity representing a sand-blasted Inconel alloy, which lines the manifolds; the small thermal resistance of the metal liner is ignored in the thermal model. Stack and system operating parameters for this study are also listed in Table 4.

Table 3 Baseline heat transfer coefficients

	h_{HB}		
h_{manifold} (W/m^2 K)	Natural conv. (W/m^2 K)	Forced conv. (W/m^2 K)	h_{amb} (W/m^2 K)
29	2	5	16

Table 4 System emissivity values and operating parameters

Emissivity values	
Interconnect	0.80
Trilayer	0.80
Manifold	0.93
Insulation	0.90
SOFC stack parameters	
N_{cells}	45
P(kPa)	228
V_{cell}(V)	0.959
j_{avg}(A/cm^2)	0.258
$\Delta T_{\text{cathode}}$(°C)	115
$T_{\text{fuel,in}}$(°C)	650
T_{cell}(°C)	800
U_F	0.85
P_{gross}(kW)	1.11
System parameters	
T_{amb}(°C)	20
P_{amb}(kPA)	202
Oxidant	Pure O_2
Fuel	Dodecane
CPOx: O/C	1.0

6 Results

Three system cases (A–C) are explored. The first (case A) is a thermal system model where recuperator exhaust gases are circulated within the hot box enclosure, resulting in forced convection within the enclosure. The second (case B) is a thermal system model where recuperator exhaust gases are directly plumbed out of the enclosure, resulting in natural convection within the enclosure. Finally, thermally coupled system model results are compared against a quasi-adiabatic system model that does not incorporate the system or stack thermal models (case C).

6.1 Case A: Thermally Integrated System Model With Forced Convection. A system statepoint diagram detailing results from a SOFC system operating from liquid dodecane ($C_{12}H_{26}$) and oxygen at the baseline conditions outlined in Tables 3 and 4 is shown in Fig. 12. Of particular interest is the temperature increase between oxidant entering the stack module and that entering the cathode compartment of the stack itself, 58°C. At the stack's operating condition of $T_{cell}=800°C$, a relatively cold oxidant stream at 652°C is required to enter the oxidant inlet manifold of the stack. The solid stack remains relatively hot at the oxidant inlet, 756°C, which presents a large temperature driving force for heat transfer to manifold cavity gases entering the stack module. A large temperature driving force does not exist at the oxidant outlet of the stack because the temperature difference between the stack and oxidant flow decreases in the direction of oxidant flow. Oxidant leaving the stack rejects heat to the manifold walls, but the magnitude of the heat rejection is small in comparison to the energy gained by oxidant gases in the stack inlet manifold.

In this system, enclosure cavity gases gain 301 W of thermal energy from the system components within. The amount of heat transfer to cavity gases is among the largest thermal energy transfers occurring in the system. The high magnitude of heat transfer from system components to the cavity gas implies that recuperator exhaust gas circulation has a major effect on system-level operating conditions.

Of the 235 W leaving the stack, 177 W or 75% is transferred via radiation to the enclosure inner wall. This reveals radiation as a substantial heat transfer mechanism in the hot box; therefore, inclusion of radiation in the system thermal model is essential. Finally, to justify the thermodynamically calculated CPOx exhaust heat loss, it is assumed that this flow occurs in a 1.25 cm diameter pipe. A tube length of 10 cm is required to shed the 148 W of required heat. This is a workable design with coiled piping connecting the CPOx to the anode manifold inlet fitting on the stack.

6.2 Case B: Thermally Integrated System Model With Natural Convection. A variation on the physical SOFC system is explored where the recuperator exhaust gas is not forced into the hot enclosure but is instead convected out of the system through conduit, as shown in the statepoint diagram of Fig. 13. All other parameter (except h_{HB}) from the forced convection case are held constant. Without the relatively cold recuperator exhaust gas entering the hot box cavity and absorbing energy, the hot box inner wall temperature is 144°C higher than with circulating recuperator exhaust gas. A higher hot box wall temperature points to lower

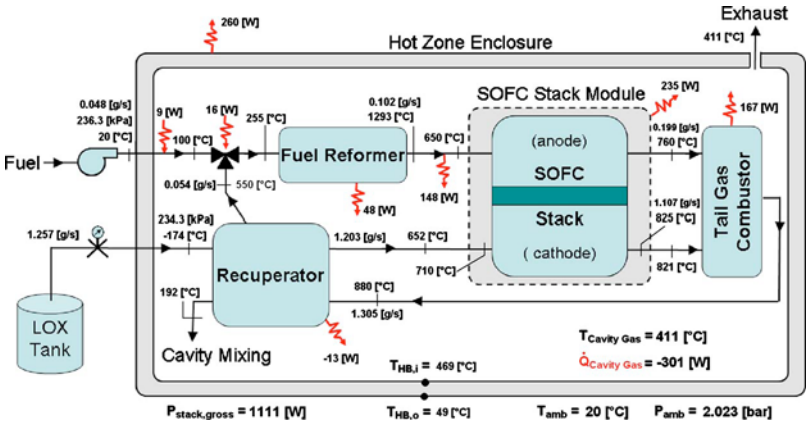

Fig. 12 Case A: thermally integrated SOFC system with recuperator exhaust gas circulation

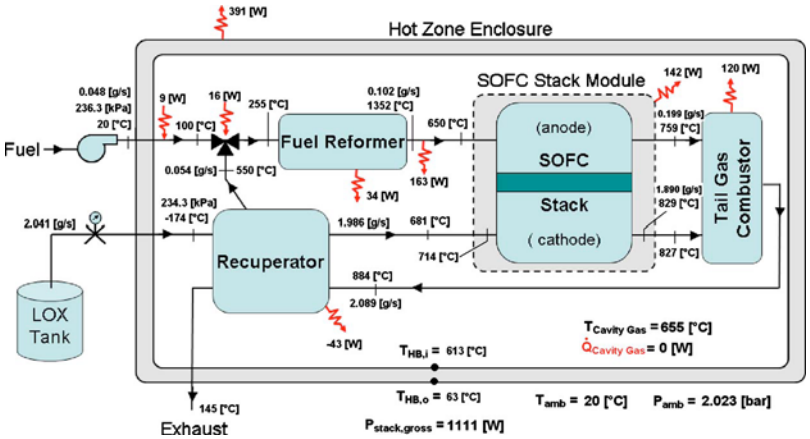

Fig. 13 Case B: thermally integrated SOFC system without recuperator exhaust gas circulation

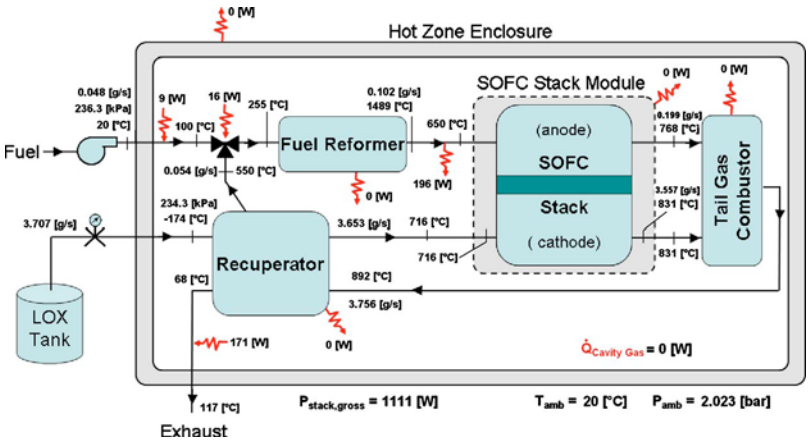

Fig. 14 Case C: thermodynamic SOFC system with quasi-adiabatic conditions

system component heat losses, which is evident in the stack because a higher oxidant flow rate is required to cool the stack. Stack oxidant flow at 1.986 g/s is 1.65 times higher than the predicted oxidant requirement with circulating recuperator exhaust gas in the enclosure (case A).

6.3 Case C: Thermodynamic System Model With Quasi-Adiabatic Conditions. To compare the coupling of the thermal model to the thermodynamic system model, an adiabatic thermodynamic system model was run at the same operating conditions used for Fig. 13. The adiabatic thermodynamic model assumes zero heat transfer from the recuperator, CPOx reformer, and burner. Stack cooling only occurs through convective gas cooling from anode and cathode streams. The two thermodynamically required heat transfers that cool CPOx reformate and preheat fuel are still allowed, with the remaining CPOx reformate heat loss added to recuperator exhaust gases. A statepoint diagram for the adiabatic system model is shown in Fig. 14. The adiabatic model predicts a required oxidant flow rate of 3.653 g/s, which is 1.84 times greater than predicted in case B and 3.04 times greater than case A. Oxidant usage becomes extremely important in mobile applications where oxidant must be stored onboard. The sensitivity of oxidant flow rate to system heat transfer predictions provides strong evidence for the need to employ thermally integrated system models.

The temperature rise of oxidant across the stack module varies for all three cases. Temperature increases of 169°C, 146°C, and 115°C in cases A, B, and C, respectively, illustrate the sensitivity of oxidant temperature rise across the stack module to system configuration and thermal model implementation. A significant fraction of oxidant heating occurs in the inlet manifold where 34% and 23% of the overall heating across the stack module occurs in the inlet manifolds of cases A and B, respectively. Oxidant heating within the stack module is also sensitive to the heat transfer coefficient used within the manifolds. A 10% reduction in h_{man} in case A lowers oxidant temperature rise by 5°C across the inlet manifold and across the stack module.

6.4 Effect on Cell Temperature Profile. Understanding the impact of thermal management on the temperature distributions within the cell-stack is another important consideration when evaluating system-level thermal interactions associated with SOFC technology. The effect of system configuration (cases A and B) and modeling approach (case C) on the solid trilayer temperature profile within the stack is shown in Fig. 15. The greatest effect of thermal integration on cell temperature is seen at the oxidant outlet to the stack where the cell temperature is lowered by about 8°C. Moving from the oxidant outlet, cell temperatures are relatively insensitive to the thermal integration method with temperatures remaining within 4°C of one another at cell positions of about 1.5–10 cm.

A greater effect on stack design and operation is shown in Fig. 16, which depicts the effect of coupled heat transfer on the solid trilayer temperature gradient. Stack temperature gradients generate thermally induced stresses. The magnitude and location of the largest gradient in the cell is important in avoiding deleterious operating conditions and in designing stacks for maximum operating life.

The overall temperature gradient profile and maximum is altered when the thermal model is integrated. The adiabatic stack

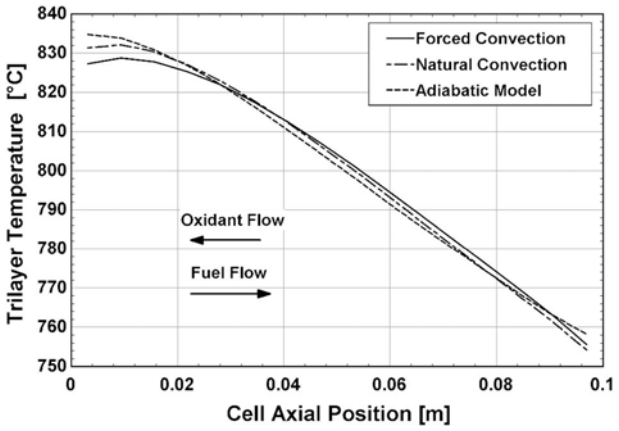

Fig. 15 Solid cell temperature profiles

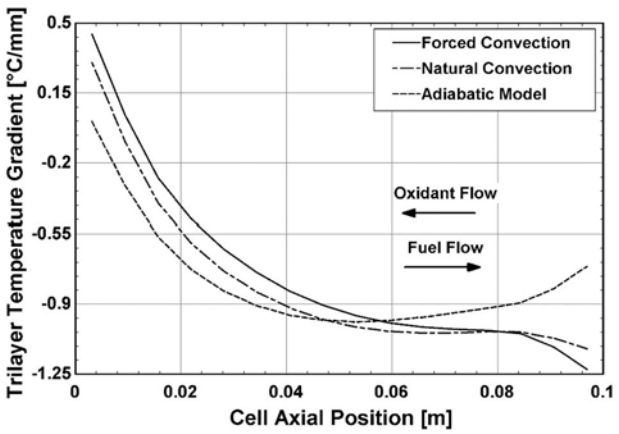

Fig. 16 Solid cell temperature gradient profiles

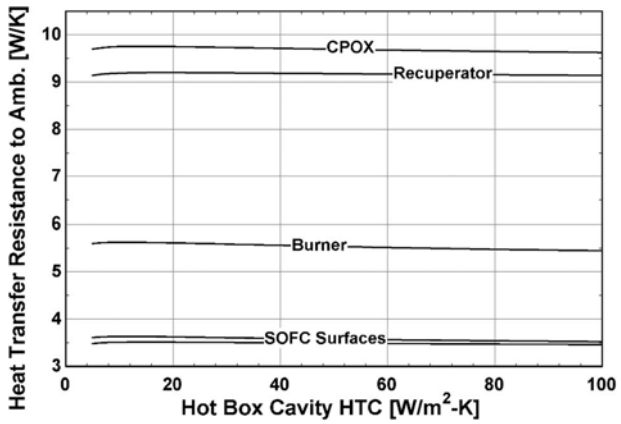

Fig. 17 Heat transfer resistances to ambient versus enclosure cavity gas heat transfer coefficient

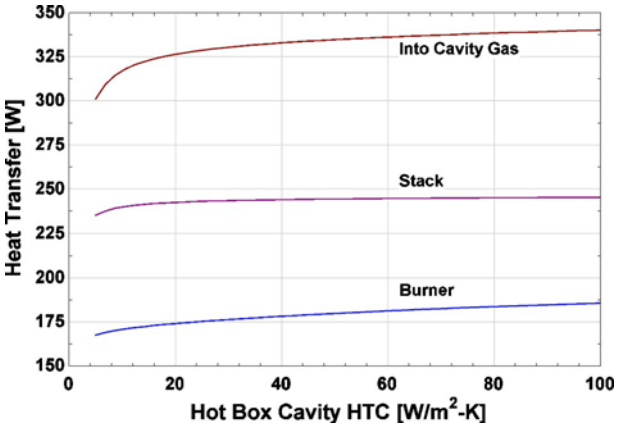

Fig. 19 Enclosure heat transfer versus enclosure cavity gas heat transfer coefficient

has a concave up distribution with a maximum gradient occurring in the interior of the cell. The thermally integrated stack model shows an inflection point in the temperature gradient distributions with the maximum gradient occurring at the cooling oxidant gas inlet to the stack rather than within the interior. The maximum cell temperature gradient is predicted to be 24% higher with a thermally integrated stack (case A) compared with an adiabatic stack model (case C).

6.5 Parametric Study on Case A: Thermally Integrated SOFC Model With Forced Convection. Now focus is shifted to the circulating recuperator exhaust gas system integrated with the thermal system model. The sensitivity of the SOFC system to the design/operating parameters h_{HB} and h_{amb} is explored in the following.

First, the sensitivity to the convective heat transfer coefficient in the enclosure cavity h_{HB} is explored as h_{HB} can be varied by installing an induced draft fan in the system outlet duct. The total thermal resistance of each BoP component, as defined in Eq. (15) along with the total resistance of the stack surfaces, is plotted against h_{HB} in Fig. 17. Interestingly, total resistance increases slightly as h_{HB} increases from 2 $\text{W/m}^2\,\text{K}$ to around 18 $\text{W/m}^2\,\text{K}$. Further increases in h_{HB} result in only slight decreases in the thermal resistance of the BoP components. The increase in resistance is due to the competition between radiation and convection heat transfer in the hot box. Increases in h_{HB} act to decrease component surface temperatures and increase radiation heat transfer resistance. The balance between radiation and convection heat transfer mechanisms in the hot box is illustrated in Fig. 18 using the burner.

Total thermal resistances show little sensitivity to h_{HB} but shown in Fig. 19 is the effect of h_{HB} on heat transferred to the recuperator exhaust cavity gases. At the lower bound, a slight increase in h_{HB} substantially increases the component heat rejection to circulating cavity gases. The large increase in heat transfer to the gas flow in the enclosure is the main reason for lower system temperatures and therefore, a higher radiation resistance. Although total resistances increase, component level heat losses increase throughout the range of h_{HB}, also shown in Fig. 19. The greatest increase in heat loss occurs in the lower h_{HB} range where heat transfer to cavity gases increases rapidly, which provides a large sink of thermal energy for system components.

As seen earlier, oxidant flow rate is highly sensitive to the implementation of the thermal model. The sensitivity of oxidant flow rate to h_{HB} is explored in Fig. 20. Oxidant flow rate shows a strong nonlinear relationship to the enclosure heat transfer coefficient below about 40 $\text{W/m}^2\,\text{K}$. The required oxidant flow into the stack decreases by nearly 7% as h_{HB} increases from 5 $\text{W/m}^2\,\text{K}$ to 40 $\text{W/m}^2\,\text{K}$. As h_{HB} increases, the stack has a decreased need for convective cathode gas cooling, as a greater fraction of thermal energy is being transferred from the stack surfaces to the enclosure and cavity gas.

Variation of the heat transfer coefficient on the outer surface of the enclosure, h_{amb}, was also explored. In the UUV application, h_{amb} is a function of the UUV's speed. Figure 21 illustrates that oxidant gas flow is less sensitive to h_{amb} than h_{HB}. The large surface area of the enclosure compared with system components

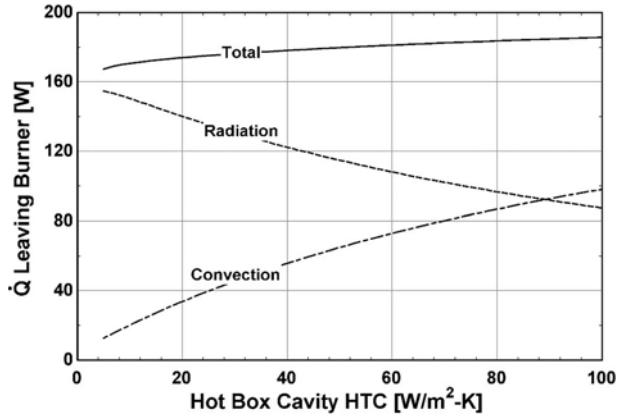

Fig. 18 Heat transfer from burner versus enclosure cavity gas heat transfer coefficient

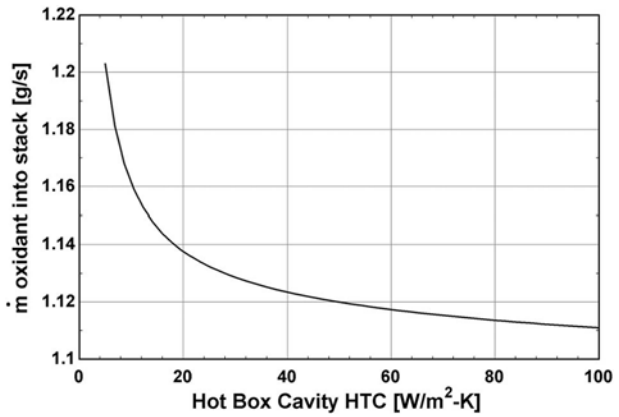

Fig. 20 Sensitivity of oxidant flow rate to enclosure cavity heat transfer coefficient

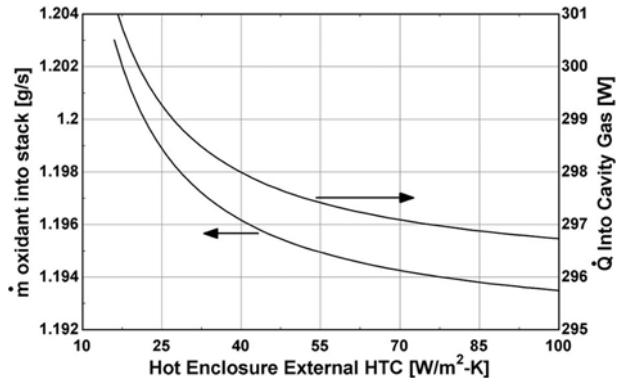

Fig. 21 Effect of external heat transfer coefficient to surroundings on system operating conditions

leads to a relatively small thermal resistance at the enclosure external boundary; therefore, a further decrease of external resistance with increasing h_{amb} has a marginal effect on the total resistance from system components. Unlike the large increase in heat absorbed by cavity gases with increasing h_{HB}, heat absorbed by cavity gases decreases slightly with increasing h_{amb}. Cavity gas heating is a major thermal energy sink for stack components and without a substantial change of energy into the cavity gas, component heat loss remains relatively constant over the range of h_{amb}. With the component heat losses relatively constant, the amount of cathode gas convective cooling in the stack remains relatively constant, which explains the low sensitivity of oxidant flow in the stack to h_{amb}.

7 Conclusion

A system-level thermal model has been developed to add fidelity to existing thermodynamic SOFC system models. The thermal model of the SOFC system includes a reformer, burner, recuperator, and SOFC stack, which are contained within a hot enclosure. Thermal interactions occur between system components as each component is coupled to both the enclosure inner wall and the circulating cavity gas through a thermal resistance network.

In this study, the thermal model was integrated with a thermodynamic system model, which included a previously developed 1D planar stack model. The 1.1 kW SOFC system under study was adapted from design concepts intended for UUV applications. Model predictions of system heat loss aid in system-level design and operating parameter selection. As shown in this study, if a conventional adiabatic thermodynamic model (case C) is used in system design, the required stack oxidant flow rate is overpredicted by 84%, requiring a 90% larger recuperator heat duty compared with the thermally integrated system model (case B).

It was further shown that circulating recuperator exhaust gas in the hot box enclosure (case A) decreases stack oxidant usage by 39% compared with directly purging recuperator exhaust from the system (case B). A 41% reduction in recuperator heat transfer duty accompanies modifying the system to allow for circulating recuperator exhaust gases. Compared against case A, adiabatic modeling results overpredict oxidant flow rate by 204% and recuperator heat duty by 221%. With circulating recuperator exhaust (case A), stack oxidant requirements and recuperator heat transfer duty drop an additional 7% by increasing the convective heat transfer coefficient in the enclosure from 5 $W/m^2 K$ to 40 $W/m^2 K$, which could be accomplished with the use of a circulating fan or other means. Model predictions point to the significance of enclosure gas circulation in sizing system components and oxidant flow rates. External thermal boundary conditions are observed to have little effect on overall system operating conditions due to the large enclosure surface area in comparison to system component areas.

Alterations in both the profile of the cell temperature gradient and the maximum value of the gradient itself were observed with the thermal management model. Thermally integrated models predict maximum thermally induced cell stress to occur at the oxidant inlet rather than within the interior of the cell-stack, as predicted with the adiabatic system model. Temperature gradients from the thermally integrated model (case A) were estimated to be about 24% higher than the adiabatic model (case C). Stack temperature gradients are also influenced by the extent of oxidant heating occurring within stack manifolds. An accurate prediction of oxidant heating within the manifolds requires an accurate convective heat transfer coefficient which is highly dependent on the manifold geometry. In this study, a simplified manifold geometry was used utilizing a rectangular duct flow relationship to calculate a convective heat transfer coefficient.

The development of a low-dimensional thermal modeling tool can be quite effective in revealing important interactions between the components and their surroundings, as well as the impact on process gas temperatures and flow requirements within the system. While the implementation of thermal management modeling with system-level design tools enables a better understanding of the coupled component heat transport phenomena within high temperature planar SOFC systems, it is acknowledged that this tool must be experimentally validated. Nevertheless, in lieu of such validation, the utility of the thermal model developed herein is that substantial design and performance insights are gained without the expense, complexity, and overhead of models that employ simulations based on a three-dimensional computational fluid dynamics software.

Acknowledgment

The authors would like to thank Robert Kee for his helpful graphics in the preparation of this paper and the financial support of the Office of Naval Research under STTR Contract No. N00014-08-M-0303 and the Department of Energy's Office of Energy Efficiency and Renewable Energy under Contract No. DE-FG36-08GO88100.

Nomenclature

A = surface area (m^2)
F_{ij} = radiation view factor from surface i to surface j
h = convective heat transfer coefficient ($W/m^2 K$)
h_{rad} = linearized radiation heat transfer coefficient ($W/m^2 K$)
J = surface radiosity (W/m^2)
k = thermal conductivity ($W/m K$)
L = material thickness (m)
OD = outer diameter
$\dot{Q}$ = heat transfer rate (W)
R = thermal resistance (W/K)
T = temperature (K)
U_F = fuel utilization

Greek Letters

σ = Stefan–Boltzmann constant ($W/m^2 K^4$)
ε = emissivity
Δ = change in

Subscripts

amb = ambient
avg = average
B = burner
BoP = balance-of-plant
cav = cavity
chan = stack gas channels
comp = compression
conv = convection

CPOx = catalytic partial oxidation
fb = fiberboard
FR = fuel reformer
HB = hot box
HTC = convective heat transfer coefficient (W/m^2 K)
i = surface i, inner surface
ins = insulation
ic = stack interconnects
j = surface j
man = manifold
o = outer surface
R = recuperator
rad = radiation
ref = reformate
surf = surface
tri = stack trilayers

References

[1] Petruzzi, L., Cocchi, S., and Finschi, F., 2003, "A Global Thermo-Electrochemical Model for SOFC Systems Design and Engineering," J. Power Sources, **118**, pp. 96–107.

[2] Lu, N., Li, Q., Sun, X., and Khaleel, M. A., 2006, "The Modeling of a Stand-Alone Solid-Oxide Fuel Cell Auxiliary Power Unit," J. Power Sources, **161**, pp. 938–948.

[3] Apfel, H., Rzepka, M., and Stimming, U., 2006, "Thermal Startup Behavior and Thermal Management of SOFCs," J. Power Sources, **154**, pp. 370–378.

[4] Lisbona, P., Corradetti, A., Bove, R., and Lunghi, P., 2007, "Analysis of Solid Oxide Fuel Cell System for Combined Heat and Power Applications Under Non-Nominal Conditions," Electrochim. Acta, **53**, pp. 1920–1930.

[5] Beale, S. B., 2005, "A Distributed Resistance Analogy for Solid Oxide Fuel Cells," Numer. Heat Transfer, Part B, **47**, pp. 573–591.

[6] Chen, Y., and Evans, J., 1996, "Cool-Down Time of Solid Oxide Fuel Cells Intended for Transportation Application," J. Power Sources, **58**, pp. 87–91.

[7] Damm, D. L., and Fedorov, A. G., 2006, "Reduced-Order Transient Thermal Modeling for SOFC Heating and Cooling," J. Power Sources, **159**, pp. 956–967.

[8] Braun, R. J., 2002, "Optimal Design and Operation of Solid Oxide Fuel Cells for Small-Scale Stationary Applications," Ph.D. thesis, University of Wisconsin, Madison, WI.

[9] Braun, R. J., Klein, S. A., and Reindl, D. T., 2006, "Evaluation of System Configurations for Solid Oxide Fuel Cell-Based Micro-Combined Heat and Power Generators in Residential Applications," J. Power Sources, **158**, pp. 1290–1305.

[10] Ackermann, T., De Haart, L. G. J., Lehnert, W., and Thom, F., 2000, "Modelling of Mass and Heat Transport in Thick-Substrate Thin-Electrolyte Layer SOFCs," Proceedings of the Fourth European SOFC Forum, Luzerne, Switzerland.

[11] Incropera, F., DeWitt, D., Bergman, T., and Lavine, F., 2007, *Fundamentals of Heat and Mass Transfer*, 6th ed., Wiley, New York.

[12] Microtherm International Ltd., 2001, "Microtherm Insulation Product and Performance Data," Product Brochure Table 3, p. 5.